Research Article Vol. 15, No. 6 / 1 Jun 2024 / Biomedical Optics Express 3743
Biomedical Optics EXPRESS

High-sensitivity THz-ATR imaging of cerebral ischemia in a rat model

HAIBIN LI,[1,2] YUYE WANG,[1,2,4] ZELONG WANG,[1,2] NING MU,[3] TUNAN CHEN,[3,5] DEGANG XU,[1,2] HUA FENG,[3] AND JIANQUAN YAO[1,2]

[1] *School of Precision Instruments and Optoelectronics Engineering, Tianjin University, Tianjin 300072, China*
[2] *Key Laboratory of Optoelectronic Information Technology (Ministry of Education), Tianjin University, Tianjin 300072, China*
[3] *Department of Neurosurgery and Key Laboratory of Neurotrauma, Southwest Hospital, Third Military Medical University (Army Medical University), Chongqing 400038, China*
[4] *yuyewang@tju.edu.cn*
[5] *ctn@tmmu.edu.cn*

Abstract: The fast label-free detection of the extent and degree of cerebral ischemia has been the difficulty and hotspot for precise and accurate neurosurgery. We experimentally demonstrated that the fresh cerebral tissues at different ischemic stages within 24 hours can be well distinguished from the normal tissues using terahertz (THz) attenuated total reflection (ATR) imaging system. It was indicated that the total reflectivity of THz wave for ischemic cerebral tissues was lower than that for normal tissues. Especially, compared to the images stained with 2,3,5-triphenyl tetrazolium chloride (TTC), the ischemic tissues can be detected using THz wave with high sensitivity as early as the ischemic time of 2.5 hours, where THz images showed the ischemic areas became larger and diffused as the ischemic time increasing. Furthermore, the THz spectroscopy of cerebral ischemic tissues at different ischemic times was obtained in the range of 0.5-2.0 THz. The absorption coefficient of ischemic tissue increased with the increase of ischemic time, whereas the refractive index decreased with prolonging the ischemic time. Additionally, it was found from hematoxylin and eosin (H&E) staining microscopic images that, with the ischemic time increasing, the cell size and cell density of the ischemic tissues decreased, whereas the intercellular substance of the ischemic tissues increased. The result showed that THz recognition mechanism of the ischemia is mainly based on the increase of intercellular substance, especially water content, which has a stronger impact on absorption of THz wave than that of cell density. Thus, THz imaging has great potential for recognition of cerebral ischemia and it may become a new method for intraoperative real-time guidance, recognition in situ, and precise excision.

1. Introduction

Cerebral ischemia is a condition in which blood flow either drops to zero or proceeds at severely decreased levels that cannot supply sufficient oxidizable substrates to maintain energy metabolism in vivo. As ischemia occurs, the collapse of cerebral energy state is usually accompanied by a series of subtle changes in anaerobic metabolism, ion, and water homeostasis that eventually initiate destructive internal and external processes in brain tissue, like the rapid death of neurons within the immediate territory of the affected artery. It is estimated that cerebral ischemia with a more or less pronounced regional reduction of perfusion is the cause of about 60~70% of all cases of acute stroke. Especially, the region of cerebral ischemia usually includes the infarct core and the ischemic penumbra. Unlike the infarct core, the penumbral area still remains structurally and metabolically intact, which has the opportunity to be functional recovery [1]. In the last few years, clinical studies have shown that the time window for the initiation of effective therapy

#524466 https://doi.org/10.1364/BOE.524466
Journal © 2024 Received 21 Mar 2024; revised 26 Apr 2024; accepted 7 May 2024; published 15 May 2024

Biomedical Optics EXPRESS

might be as short as 3 h to obtain the highest possible benefit [2–4]. If the time is prolonged, the risk of permanent tissue damage is increased. Perfusion coherence tomography (CT) has been shown to have a sensitivity of 90% and a specificity of 100% to accurately detect the type and extent of the underlying ischemic process, but the major disadvantage of CT scan is the exposure to ionizing radiation [5–7]. Of note, perfusion imaging requires the use of a contrast agent as a tracer to track the flow of blood. The perfusion- and diffusion-weighted magnetic resonance imaging (MRI) provide similar information with greater sensitivity and specificity based on the basic principles of measuring cerebral blood flow and water molecule movement, respectively [8,9]. Multiparametric modes incorporating information from various CT and MRI sequences have been proposed to improve the prediction accuracy of these compartments [10]. However, these approaches have some limitations, such as inhomogeneous static magnetic field-induced distortion, the necessity of special coils, high cost, and time-consuming. And the intraoperative implementation is complex. Most up-to-date intraoperative technologies for monitoring the regional cerebral blood flow (CBF) and cerebral electrical activity [11], including thermal diffusion flowmetry, transcranial Doppler ultrasonography, laser Doppler flowmeter, and near-infrared spectrophotometry [12], have several shortcomings, such as low reliability, poor spatial and temporal resolution, inaccuracy, and unclear biophysics mechanism. OCT imaging has been proposed to monitor ischemic injury, which is based on the scattering mechanism of structural arrangements of cells and organelles in biological tissues, but the imaging range is limited and it usually needs to be combined with complex post-processing algorithms [13]. Pathological image analysis methods are the gold standard for medical diagnosis, but they are time-consuming in general. Hence, the fast label-free detections of the extent and degree of cerebral ischemia are significant in precise and accurate neurosurgery. Therefore, more feasible methods to help doctors better diagnose the degree of ischemia during treatment are urgently needed.

Terahertz (THz) wave, located between the infrared and microwave regions of the electromagnetic spectrum, has the unique physical characteristics of non-ionizing and low photon energy. Thus, THz wave does not cause damage to biological tissues compared to other band lights such as visible light, X-rays, and gamma rays [14,15]. THz imaging is mainly dependent on the absorption mechanism in biological tissue due to its fingerprint spectrum and high sensitivity to polar molecules [16]. Until now, THz imaging techniques have been studied as candidates for biomedical imaging, such as the detection of knee cartilage [17] and skin burn [18], hepatocellular carcinoma [19], oral [20], and skin cancers [21,22], as well as intraoperative diagnosis of breast cancer [23] and brain glioma in vivo [24]. In neurosurgery field, THz spectroscopy [25,26] and imaging [27] have been tried to reveal characteristics differences between lesions and normal tissue [28]. However, THz transmission imaging requires the tissue to be sliced, while THz reflection imaging is always affected by diffuse reflection for uneven surface of samples. Attenuated total reflection (ATR) imaging can provide information on the interaction between the sample and evanescent wave traveling along a prism surface. Thus, THz-ATR imaging has been proposed to obtain the precise absorption information of sample and improve the imaging sensitivity. Moreover, with the development of solid immersion lens, the imaging area and resolution could be significantly improved [29]. Meanwhile, some data processing techniques for THz medical imaging have been developed, such as agglomerative hierarchical clustering and principal component analysis [30,31]. Therefore, THz imaging has great potential for assisting medical diagnosis, especially the recognition in situ, intraoperative real-time guidance, and precise excision. The fundamental diagnosing principle with THz wave is its sensitivity to subtle changes in tissue water content and structure. Considering the process of cerebral ischemia has a series of changes in metabolism and water homeostasis, it is suggested that THz imaging could become a possible label-free method for detecting the extent and degree of cerebral ischemia.

Biomedical Optics EXPRESS

In this paper, THz-ATR imaging of fresh rat ischemic cerebral tissues at different ischemic stages has been investigated based on continuous-wave (CW) THz imaging system operating at 2.52 THz. The ischemic cerebral tissues can be well distinguished by THz intensity imaging. Especially, the ischemic stage can be recognized as early as 2.5 hours, which shows high sensitivity compared with the visualized images stained with 2,3,5-triphenyltetrazolium chloride (TTC). Furthermore, for the better understanding the characterization of cerebral ischemic tissues in THz range, the THz spectroscopy of cerebral ischemic tissues with different ischemic times were obtained in the range of 0.5 THz to 2.0 THz by THz time-domain spectroscopy (THz-TDS) system. Additionally, histological analysis with hematoxylin and eosin (H&E) staining photography was performed to reveal whether intrinsic properties contribute to the difference in THz imaging results.

2. Methodology

2.1. Experimental setup

The schematic diagram of the THz-ATR imaging system was shown in Fig. 1(a). An optically pumped THz gas laser (FIRL100, Edinburgh Instruments Ltd.) was employed as the THz source. The frequency of 2.52 THz was chosen with output power of 50 mW. Two room-temperature-operated Golay cells (GC-1P, Tydex Ltd.) were used as the detectors. Considering the responsivity of the detectors, THz wave was modulated by a chopper (SR540, Stanford Research Systems Inc.) operating at 50 Hz. To reduce the random image noises from slight power fluctuations, a wire grid polarizer (Microtech Instruments, Inc.) was used to split the THz wave into two beams with basically the same signal intensity, whose polarization directions were horizontal and vertical to the horizontal plane, respectively. The beam with vertical polarization was the reference beam, and the horizontal beam was used as the signal beam. The reference beam was received by the Golay cell directly, which can provide the pixel reference $I_{reference}$. Here, $I_{reference}$ was used to monitor the fluctuation of the THz signals during measurement and calibrate the signal beam according to the fluctuation in reflectivity calculation. The signal beam was reflected and focused by the gold-coating mirror and off-axis parabolic mirror 1 with 30° off-axis angle. The focused signal light was incident into an isosceles triangle-shaped silicon ($n = 3.42$ at 2.52 THz) prism, whose size was $34.8 \times 34.8 \times 20$ mm^3 with base angle of 49° [32]. Then the signal beam carrying the sample information was reflected by the off-axis parabolic mirrors 2 and 3 and received by the Golay cell. The focal lengths of off-axis parabolic mirrors 1 and 2 were 2 inches with the F-number of 1, whereas the focal length of off-axis parabolic mirror 3 was 4 inches with the F-number of 2. For the refractive index of biological samples is usually smaller than that of distilled water ($n = 2.05$ at 2.52 THz), the incident angle at the prism bottom was 43.5° which was larger than the theoretical critical angle of 34.8° for distilled water. The prism and objective table were both mounted on a two-dimensional (2-D) motor stage (Sigma Koki Co., Ltd.). Sample was placed on the objective table and its upper surface was in close contact with the prism bottom surface where the focus of the signal light was located. Considering the sample and prism were scanned simultaneously, the contact of the prism with sample can be well maintained during the imaging process. Although such a process causes some movement or extrusion of the local tissue within 1 mm, it is acceptable in neurosurgery. The resolution of the THz-ATR imaging system was 400 μm × 440 μm using agar scanning which was shown in Fig. 1(b). The scanning speed was about 10 pixels/s with the scanning step of 200 μm in this study. The experiment was done under a controlled room temperature.

To investigate the spectroscopy of ischemic cerebral tissues in THz range, a commercially available THz time-domain spectroscopy (TDS, Advantest Corp., TAS7500SP) in transmission geometry was used. The spectrum reached over 2.0 THz from 0.5 THz, with the frequency resolution and spatial resolution of 7.6 GHz and 2 mm, respectively. The measurements were performed at room temperature (23°C) with dry air purge.

Biomedical Optics EXPRESS

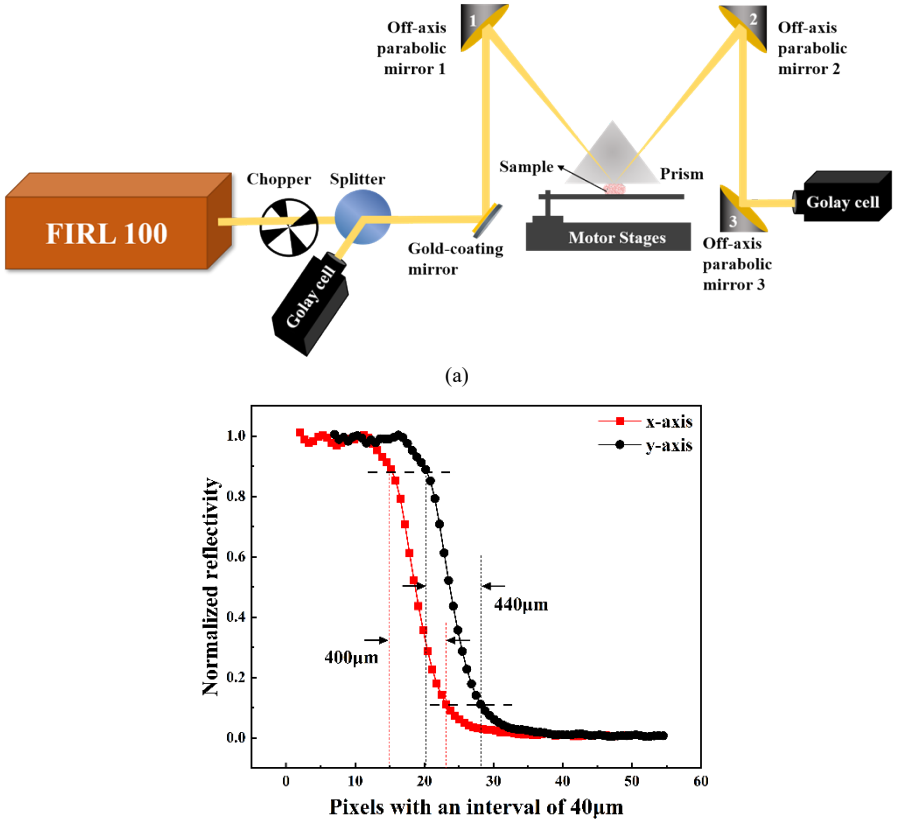

Fig. 1. (a) Continuous-wave THz-ATR imaging system; (b) the resolution of the THz-ATR imaging system.

2.2. Sample preparation and measurement protocol

To guarantee the reliability of the experiments, a reproducible measurement protocol was established by standardizing all experimental steps of sample preparations and THz measurements. The care of laboratory animals and the animal experimental operation have been conforming to the China Administration Rule of Laboratory Animal. All animal experimental protocols and euthanasia were reviewed and approved by the Laboratory Animal Welfare and Ethics Committee of the Third Military Medical University.

Fifty-six male Sprague Dawley (SD) rats weighing between 220 g and 240 g were used in this study. Permanent middle cerebral artery occlusion (MCAO) was carried out as previously reported [33]. Briefly, a midline incision was made in the neck to expose the left common carotid artery (CCA), external carotid artery (ECA), and internal carotid artery (ICA). A 4-0 monofilament suture (Shadong Biotech Corp. Ltd., Beijing, China) with a tip diameter of 0.32-0.36 mm coated with silicon was inserted into the ICA through the ECA stump to block the blood flow to the middle cerebral artery. The filament was gently advanced into the left ICA at approximately 17 mm above the carotid bifurcation until mild resistance was felt. The left side of brain tissue was set as the ischemic side. Generally, ischemia within 24 hours is usually considered as transient ischemic attack, and 3 hours after the onset of cerebral ischemia is the golden time for surgical treatment [34]. Thus, the ischemia time points of 1, 2, 2.5, 3, 4, 6, and 24 hours were prepared. The rat brains were extracted after euthanasia at 1, 2, 2.5, 3, 4, 6, and

Biomedical Optics EXPRESS

24 hours after MCAO, and the intact brain tissues were excised and preserved in oleic acid for water content preservation, where 7 rats were prepared for each ischemic point. For comparison, the same surgical procedures were also performed on 7 normal rats, which were set up as the sham group. Among the 7 rats in each group, 2 rats were used for TTC staining, 2 rats were used for H&E staining, and 3 rats were used for THz-ATR imaging detection and THz spectral detection of tissue slices. Generally, cerebral ischemia is visualized by staining brain slices with TTC (Sigma-Aldrich). Normal tissue areas turn red due to internal dehydrogenase interacting with TTC, whereas ischemic areas are unable to interact with TTC due to inactivation of internal dehydrogenases, resulting in a white coloration. Besides, the intrinsic properties of cerebral tissues can be detected using H&E staining photography. The freshly excised brain tissues of different cerebral ischemic times were sectioned into a series of 20-μm-thick slices for H&E staining and the images were obtained by a phase-contrast microscope. The average cell density, cell size as well as intercellular substance were quantified by the ImageJ plugin 'Cell counter'. The measurements were replicated and the data was recorded for subsequent statistical analysis. For the samples of THz-ATR imaging and THz spectroscopy measurement, the samples were sliced from the coronal surface by the microtome (Leica, CM1950) to ensure that the surface remains relatively flat. Moreover, 3 tissue slices from each rat with the thickness of 70 μm were used for THz spectroscopy measurement.

2.3. Data analysis

For THz imaging, in order to reduce the image noises from slight power fluctuations, the reflected THz beam by beam splitter and the transmitted THz beam were used as the reference $I_{substrate}$ and the signal I_{sample}, respectively. The image of sample was obtained with the pixel value of $I_{sample}/I_{substrate}$. The THz imaging with and without sample were measured as the images of F_{sample} and $F_{substrate}$, respectively. Considering the uniformity of the ATR prism, the total reflectivity R of sample can be obtained with the pixel values of $F_{sample}/F_{substrate}$ [32].

For THz spectroscopy measurement, two overlapped blank quartz windows were placed in the optical path to collect the reference signal. After that, the brain tissue sample sandwiched between two quartz windows was placed at the focus of the THz beam to collect the sample signal. For each rat sample, 6 slices were prepared for the detection. The time-domain THz pulses were collected at three different spots in ischemic hemisphere for each sample. Every measurement point was repeatedly tested 3 times with the setting of 1024 times scan for each measurement. Due to the biological diversity, all spectra were averaged results of 3 rat samples and the standard deviation was shown as error bars. After completing the signal acquisition, the fast Fourier transform of the time-domain signal was performed to obtain the frequency-domain spectroscopy. The absorption coefficient $\alpha(\omega)$ and the refractive index $n(\omega)$ can be calculated with Eqs. (1)–(2) [35],

$$n(\omega) = 1 - T(\omega) \cdot \frac{c}{\omega d} \tag{1}$$

$$\alpha(\omega) = -\frac{2}{d} \cdot \ln\left\{|T(\omega)| \cdot \frac{[1 + n(\omega)] \cdot [n_{sub} + n(\omega)]}{2n(\omega) \cdot (1 + n_{sub})}\right\} \tag{2}$$

Here, c is the velocity of light in vacuum, d is the sample thickness, n_{sub} is the refractive of the substrate, and $T(\omega)$ is the sample transfer function. These parameters have significant physical interpretations and are commonly used to distinguish between normal and diseased tissues [36,37].

Biomedical Optics EXPRESS

3. Results and discussion

3.1. THz image of fresh cerebral ischemic tissues

To study the THz characteristics of the fresh cerebral ischemic tissues, we measured the fresh rat tissues at different ischemic stages (1, 2, 2.5, 3, 4, 6, and 24 hours) and the normal rat brain samples (indicated as 0 hour) by THz-ATR imaging system. Figure 2 shows the TTC-stained images and THz images of the fresh cerebral tissues of the rats. From the TTC-stained images in Fig. 2(a)-(d), it is seen that there was no clear pale area observed in the cerebral tissues in the first ischemic 2.5 hours. In the TTC-stained image of Fig. 2(e), a small pale area emerged on the left side at the ischemic time of 3 hours. In the TTC-stained images of Fig. 2(f)-(h), the pale area increased gradually from the ischemic time of 4 hours to 24 hours, which can indicate the ischemic area was enlarged. In the THz images, different colors represented the change of the total reflectivity of THz wave of samples, where these THz images have the same color bar. As shown in the THz images of Fig. 2(a)-(h), the THz total reflectivity of brain tissues with different ischemic degrees ranged from 31% to 43%. Among them, Fig. 2(a) is the THz image of normal brain tissue, where the average total reflectivity was about 43% and image distribution was relatively uniform. As ischemia time prolonged to, the green and yellow colors appeared, as shown in Fig. 2(a)-(c). Then, when the ischemic time reached 2.5 hours, red areas with average total reflectivity less than 41.4% emerged in Fig. 2(d). Subsequently, the yellow and red areas in THz images gradually expanded as the increase of ischemic time, which indicated the total reflectivity of both left and right brain tissues decreased. When the ischemic time reached 24 hours, the red areas occupy nearly half of the sample, and most areas of the sample have total reflectivity close to 30%, which conforms to the characteristic of left brain ligation of ischemic model.

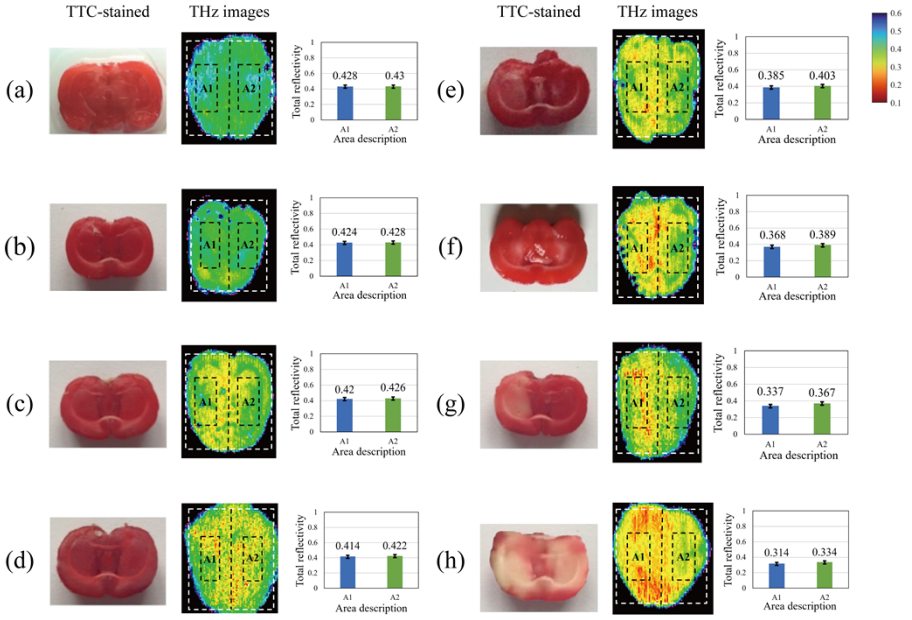

Fig. 2. The TTC-stained images and the THz images of fresh cerebral ischemic tissue samples with different ischemic times. In THz images, some areas are marked by a dashed line, and the average total reflectivity of these areas was described in the right image. The ischemic times of cerebral samples were (a) 0 hour, (b) 1 hour, (c) 2 hours, (d) 2.5 hours, (e) 3 hours, (f) 4 hours, (g) 6 hours, (h) 24 hours, respectively.

Biomedical Optics EXPRESS

In order to further analyze the THz characteristics of cerebral ischemic tissues, the total reflectivity in THz images of 24 samples were analyzed. Firstly, the enclosing rectangular region of THz images of brain tissue, depicted by white dotted line, was divided into two equal sub-regions on the left and right sides. The length of the rectangular region was set to L and the width was set to W. Thus, the area of each sub-region was $\frac{1}{2}L \times W$. The intermediate region with the area of $\frac{1}{2}(\frac{1}{2}L \times W)$ of each sub-region was selected, which was marked by black dotted line. Then, the average total reflectivity of each intermediate region, namely the ischemic hemisphere sub-region A1 and non-ischemic hemisphere sub-region A2, was calculated, which was shown in the right side of Fig. 2. Overall, the total reflectivity in A1 and A2 decreased significantly with ischemia time increasing, and the difference between A1 and A2 at certain ischemia time shows different trend.

Furthermore, the total reflectivity of 3 samples at each ischemic time was calculated respectively and averaged to analyze the relationship between total reflectivity in different hemisphere regions, as shown in Fig. 3. The total reflectivities in the ischemic hemisphere A1 and the non-ischemic hemisphere A2 decreased significantly after 2.5 hours of ischemia. When the ischemic time reached 24 hours, the total reflectivity in ischemic hemisphere A1 decreased by 11.4%, while it decreased by 9.6% in non-ischemic hemisphere. The results indicate that THz imaging can effectively reflect the difference between normal tissue and ischemic tissue through the change of reflectivity, where the reflectivity of ischemic tissues show clear decreasing trend with the increase of ischemic time. It can be attributed to that the degree of edema gradually became serious with the time increase, which lead to the THz absorption enhancement.

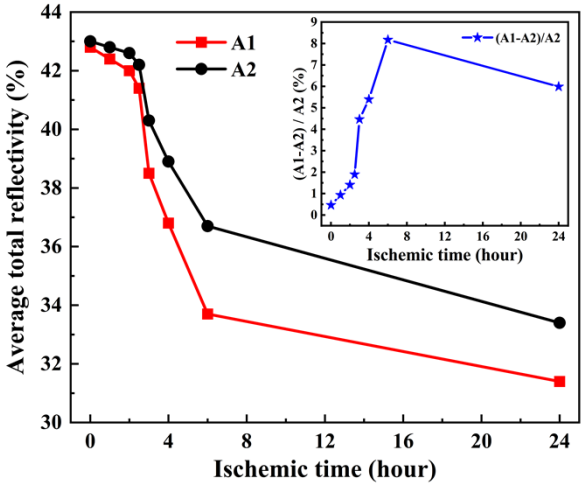

Fig. 3. The average total reflectivity of THz wave in the areas A1 and A2, and their differences within ischemic 24 hours.

Additionally, the relative difference of average total reflectivity for THz wave in areas A1 and A2 within 24 hours was shown in the inset diagram of Fig. 3. The relative difference in reflectivity between the left and right brain within 2 hours was less than 1.5%. From 3 hours of ischemia, the relative difference between the left and right brain increased suddenly, which reached the maximum of 8.17% at 6 hours. When the ischemia time reached 24 hours, the reflectivity difference between the left and right brain regions decreased to 5.98% due to the reflectivity of left and right brain both decreased. This is mainly due to the fact that, as the ischemia time increased, the ischemic range with low reflectivity expanded from the left hemisphere to the right hemisphere, which coincided with the results presented in TTC-stained images.

Biomedical Optics EXPRESS

3.2. THz spectra of fresh cerebral ischemic tissues

For the better understanding the spectral characteristics of cerebral ischemic tissue in THz range, the spectra of 24 fresh cerebral ischemic tissue samples were measured. Considering the spatial resolution of THz-TDS system was 2 mm, the brain tissue was sliced to ensure that the light spot can totally cover the ischemic region or normal region. In order to avoid water loss and other errors during sample measurement, the tissue with 70 μm thickness was sandwiched by two quartz plates and wrapped with vaseline and oleic acid [24]. The time-domain THz pulses were collected at three different spots in ischemic regions for each sample. Every measurement point was repeatedly tested 3 times with the setting of 1024 times scan for each measurement. Due to the biological diversity, all spectra were averaged results of samples and the standard deviation was shown as error bars.

Figure 4(a) and (b) show the absorption coefficient spectra and the refractive index spectra of ischemic regions in freshly brain tissue samples with different ischemic times, respectively. As shown in Fig. 4(a), steady increasing of the absorption coefficients for brain samples from all groups were observed when the frequency increased from 0.5 THz to 2.0 THz. The absorption coefficient of sham group was lower than that of ischemic groups in 0.5-2.0 THz. Especially, the absorption coefficient was positively correlated with the increasing of ischemic time. On the contrary, it can be clearly seen from Fig. 4(b) that the refractive index of all groups was decreased when the frequency increased from 0.5 THz to 2.0 THz. The refractive index of sham group was higher than that of ischemic groups in 0.5-2.0 THz, and the refractive index decreased with the increase of ischemia time. Overall, the discrepancy of absorption coefficient and the refractive index between ischemia group and sham group increased with the THz frequency increasing. In order to observe the temporal changes more clearly, the normalized absorption coefficient and refractive index values at 1.4 THz were selected as an examaple, as shown in Fig. 4(c). At each time node, the normalized values were obtained through dividing the absorption coefficient and refractive index by the value of the sham group, which can indicate the relative difference of absorption coefficient and refractive index between the control group and each ischemic group more intuitively. With the increasing of ischemic time, the normalized absorption coefficients began to rise gradually and reached the maximum at 24 h. Accordingly, the trend of normalized refractive index in THz range was opposite to that of absorption coefficient, which decreased corresponding the ischemic time.

In order to further analyze the reason for the difference in the absorption of THz waves by tissues with different degrees of cerebral ischemia, the extra 2 rats were tested for pathology, where the comsumed time was similar to that in THz imaging and spectroscopy detection. H&E-stained microscopic images (×400) were obtained from the ischemic cerebral tissues of the rats at 1, 2, 2.5, 3, 4, 6, and 24 hours after the induction of MCAO, as shown in Fig. 5(a)-(h). Based on H&E-stained images, the cell size, cell density and the intercellular substance of brain tissue samples at different ischemic time were counted separately by Image J, where the data was the averaged results from two rat samples at each time and the standard deviation was shown as error bars. The results showed that the cell size and density gradually decreased with time extension, which were shown in Fig. 5(i) and (j). On the contrary, the intercellular substance of the samples, including cell fiber, extracellular matrix, and fluid substances such as water-rich tissue fluid and lymph, increased with time, as shown in Fig. 5(k). Especially, the cell structure of brain tissue was destroyed obviously after 24 hours of ischemia. Until now, current research has shown that the absorption of THz wave by dehydrated tissues was mainly affected by cell density [38]. The greater the cell density, the greater the absorption coefficient. However, comparing the relationship between the intercellular substance and THz absorption coefficient and refractive index, it is known that the THz absorption of fresh cerebral ischemic tissue is mainly affected by water content. Due to the high THz wave absorption of water, the THz absorption coefficient increased as ischemic time prolonged. Moreover, due to the increasing of intercellular substance,

Biomedical Optics EXPRESS

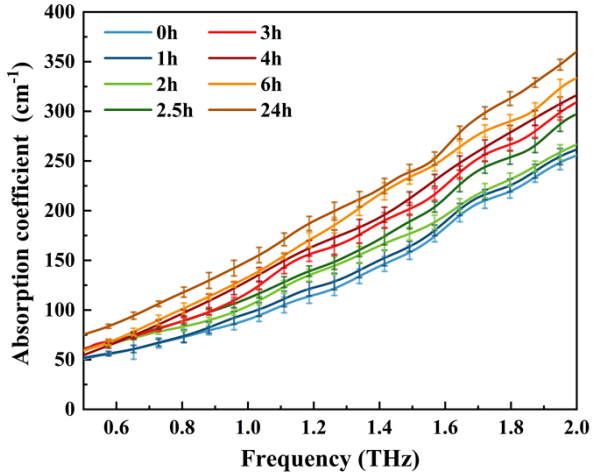

(a)

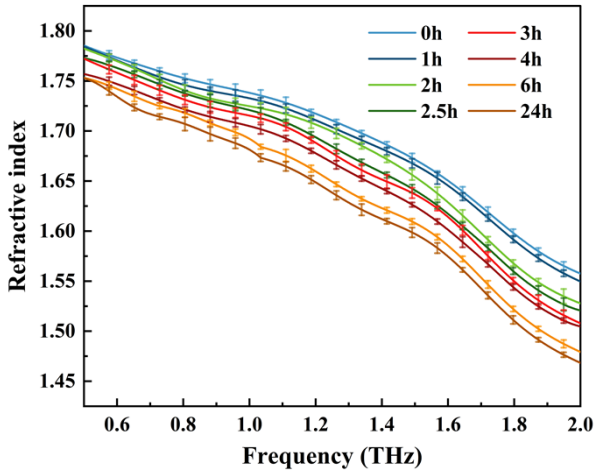

(b)

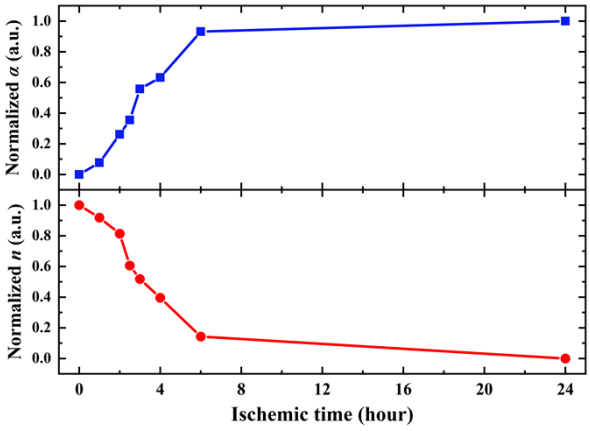

(c)

Fig. 4. (a) The absorption coefficient of fresh cerebral tissue samples at different ischemic time, (b) the refractive index of fresh cerebral tissue samples at different ischemic time, (c) the normalized absorption coefficient and refractive index values at 1.4 THz.

Biomedical Optics EXPRESS

especially the water-rich tissue fluid, the refractive index of THz wave decreased, which showed the similar trend of THz spectroscopy of water [39].

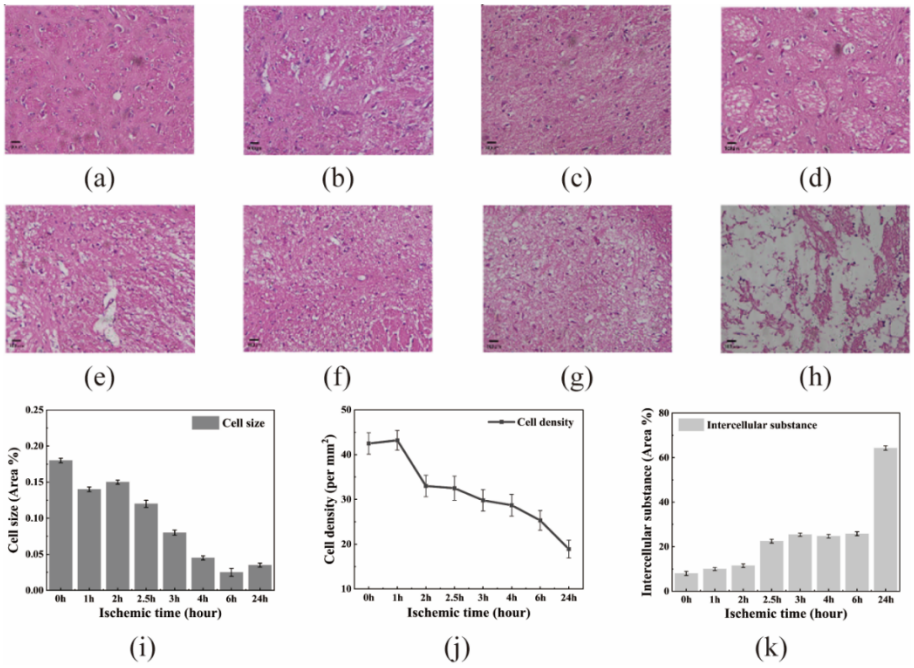

Fig. 5. (a)-(h): H&E-stained microscopic images (×400) of fresh cerebral ischemic tissues. The ischemic times of the cerebral samples are (a) 0 hour, (b) 1 hour, (c) 2 hours, (d) 2.5 hours, (e) 3 hours, (f) 4 hours, (g) 6 hours, (h) 24 hours, respectively. i-k: quantitative measurements assessed using ImageJ, (i) cell size, (j) cell density, (k) intercellular substance.

4. Conclusion

We obtained THz-ATR images of cerebral ischemic tissues from rat models by continuous-wave THz-ATR imaging system at 2.52 THz. It was demonstrated that the ischemic tissues can be detected using THz wave with high sensitivity as early as the ischemic time of 2.5 hours, where the total reflectivity of the THz wave for ischemic cerebral tissue was lower than that for normal cerebral tissues. Simultaneously, as the ischemic time increased, THz images showed the ischemic area became larger and diffused, which was in agreement with the TTC-stained images. It should be noted that THz imaging allows the ischemic zone to be visualized within an ischemic time of 2.5 hours, which is earlier than TTC-stained images. Besides, the absorption coefficients and refractive indices of fresh cerebral ischemic tissues with different ischemic time have been measured by THz-TDS system in the range of 0.5-2.0 THz. The spectral results showed that, as the ischemic time increased, the absorption coefficient of ischemic tissue increased, whereas the refractive index decreased. Additionally, the cell density has been analyzed by H&E-stained microscopic images. It is found that the cell size and cell density of the ischemic tissues decreased as the time of ischemic time increased, but the intercellular substance of the ischemic tissues increased as the time of ischemic time increased. It indicates that intercellular substance, especially water content, has a stronger impact on absorption of THz wave than that of cell density. Compared with other imaging techniques, THz imaging can realize the early identification of cerebral ischemia with the advantages of label-free and high sensitivity. In order to further realize the precise diagnosis of ischemic penumbral zone, the resolution and imaging

Biomedical Optics EXPRESS

speed of THz imaging system should be improved in the future. The unique ability of THz imaging may become a new method for intraoperative real-time guidance, recognition in situ, and precise excision.

Funding. China National Funds for Distinguished Young Scientists (62175182, 62275193, U22A20123, U22A20353).

Disclosures. The authors declare no conflicts of interest.

Data availability. Data underlying the results presented in this paper are not publicly available at this time but may be obtained from the authors upon reasonable request.

References

1. C. M. Ermine, A. Bivard, M. W. Parsons, *et al.*, "The ischemic penumbra: From concept to reality," Int. J. Stroke. **16**(5), 497–509 (2021).
2. A. Denes, R. Vidyasagar, J. Feng, *et al.*, "Proliferating resident microglia after focal cerebral ischemia in mice," J. Cereb. Blood Flow Metab. **27**(12), 1941–1953 (2007).
3. R. A. Kauppinen, "Multiparametric magnetic resonance imaging of acute experimental brain ischemia," Prog. Nucl. Magn. Reson. Spectrosc. **80**, 12–25 (2014).
4. E. Klotz and M. König, "Perfusion measurements of the brain: using dynamic CT for the quantitative assessment of cerebral ischemia in acute stroke," Eur. J. Radiol. **30**(3), 170–184 (1999).
5. C. H. P. Cremers, P. C. Vos, I. C. van der Schaaf, *et al.*, "CT perfusion during delayed cerebral ischemia after subarachnoid hemorrhage: distinction between reversible ischemia and ischemia progressing to infarction," Neuroradiology **57**(9), 897–902 (2015).
6. C. H. P. Cremers, J. W. Dankbaar, M. D. Vergouwen, *et al.*, "Different CT perfusion algorithms in the detection of delayed cerebral ischemia after aneurysmal subarachnoid hemorrhage," Neuroradiology **57**(5), 469–474 (2015).
7. D. G. Gadian, R. S. Frackowiak, H. A. Crockard, *et al.*, "Acute cerebral ischemia: concurrent changes in cerebral blood flow, energy metabolites, pH, and lactate measured with hydrogen clearance and ^{31}P and ^{1}H nuclear magnetic resonance spectroscopy. I. methodology," J. Cereb. Blood Flow Metab. **7**(2), 199–206 (1987).
8. H. A. Crockard, D. G. Gadian, R. S. Frackowiak, *et al.*, "Acute cerebral ischemia: concurrent changes in cerebral blood flow, energy metabolites, pH, and lactate measured with hydrogen clearance and 31P and 1 H nuclear magnetic resonance spectroscopy. II. changes during ischemia," J. Cereb. Blood Flow Metab. **7**(4), 394–402 (1987).
9. K. Allen, A. L. Busza, H. A. Crockard, *et al.*, "Acute cerebral ischemia: concurrent changes in cerebral blood flow, energy metabolites, pH, and lactate measured with hydrogen clearance and 31P and 1 H nuclear magnetic resonance spectroscopy. III. changes following ischemia," J. Cereb. Blood Flow Metab. **8**(6), 816–821 (1988).
10. I. M. Germano, L. H. Pitts, I. Berry, *et al.*, "High energy phosphate metabolism in experimental permanent focal cerebral ischemia: an in vivo 31P magnetic resonance spectroscopy study," J. Cereb. Blood Flow Metab. **8**(1), 24–31 (1988).
11. R. Gill, N. R. Sibson, R. H. Hatfield, *et al.*, "A comparison of the early development of ischemic damage following permanent middle cerebral artery occlusion in rats as assessed using magnetic resonance imaging and Histology," J. Cereb. Blood Flow Metab. **15**(1), 1–11 (1995).
12. D. Sauer, P. R. Allegrini, A. Cosenti, *et al.*, "Characterization of the cerebroprotective efficacy of the competitive NMDA receptor antagonist CGP40116 in a rat model of focal cerebral ischemia: an in vivo magnetic resonance imaging study," J. Cereb. Blood Flow Metab. **13**(4), 595–602 (1993).
13. W. J. Choi, Y. D. Li, and R. K. Wang, "Monitoring acute stroke progression: multi-parametric OCT imaging of cortical perfusion, flow, and tissue scattering in a mouse model of permanent focal ischemia," IEEE Trans. Med. Imaging **38**(6), 1427–1437 (2019).
14. Y. W. Fan, Q. Ma, J. Liang, *et al.*, "Quantitative and qualitative evaluation of recovery process of a 1064 nm laser on laser-induced skin injury: in vivo experimental research," Laser Phys. Lett. **16**(11), 115604 (2019).
15. Y. W. Fan, Q. Ma, M. S. Li, *et al.*, "Quantitative investigation of laser ablation based on real-time temperature variations and OCT images for laser treatment applications," Lasers Surg. Med. **54**(3), 459–473 (2022).
16. A. J. Fitzgerald, X. Tie, M. J. Hackmann, *et al.*, "Co-registered combined OCT and THz imaging to extract depth and refractive index of a tissue-equivalent test object," Biomed. Opt. Express **11**(3), 1417–1431 (2020).
17. W. C. Kan, W. S. Lee, W. H. Cheung, *et al.*, "Terahertz pulsed imaging of knee cartilage," Biomed. Opt. Express **1**(3), 967–974 (2010).
18. P. Tewari, C. P. Kealey, D. B. Bennett, *et al.*, "In vivo terahertz imaging of rat skin burns," J. Biomed. Opt. **17**(4), 040503 (2012).
19. J. Y. Park, H. J. Choi, K. S. Cho, *et al.*, "Terahertz spectroscopic imaging of a rabbit VX2 hepatoma model," J. Appl. Phys. **109**(6), 064704 (2011).
20. Y. C. Sim, J. Y. Park, K. M. Ahn, *et al.*, "Terahertz imaging of excised oral cancer at frozen temperature," Biomed. Opt. Express **4**(8), 1413–1421 (2013).
21. Z. D. Taylor, R. S. Singh, M. O. Culjat, *et al.*, "Reflective terahertz imaging of porcine skin burns," Opt. Lett. **33**(11), 1258–1260 (2008).
22. K. I. Zaytsev, K. G. Kudrin, V. E. Karasik, *et al.*, "In vivo terahertz spectroscopy of pigmentary skin nevi: Pilot study of non-invasive early diagnosis of dysplasia," Appl. Phys. Lett. **106**(5), 053702 (2015).

Biomedical Optics EXPRESS

23. H. Chen, T. H. Chen, T. F. Tseng, *et al.*, "High-sensitivity in vivo THz transmission imaging of early human breast cancer in a subcutaneous xenograft mouse model," Opt. Express **19**(22), 21552–21562 (2011).
24. L. M. Wu, D. G. Xu, Y. Y. Wang, *et al.*, "Study of in vivo brain glioma in a mouse model using continuous-wave terahertz reflection imaging," Biomed. Opt. Express **10**(8), 3953–3962 (2019).
25. A. A. Gavdush, N. V. Chernomyrdin, K. M. Malakhov, *et al.*, "Terahertz spectroscopy of gelatin-embedded human brain gliomas of different grades: a road toward intraoperative THz diagnosis," J. Biomed. Opt. **24**(02), 1–5 (2019).
26. A. A. Gavdush, N. V. Chernomyrdin, G. A. Komandin GA, *et al.*, "Terahertz dielectric spectroscopy of human brain gliomas and intact tissues ex vivo: double-Debye and double-overdamped-oscillator models of dielectric response," Biomed. Opt. Express **12**(1), 69–83 (2021).
27. H. L. Zhao, Y. Y. Wang, L. Y. Chen, *et al.*, "High-sensitivity terahertz imaging of traumatic brain injury in a rat model," J. Biomed. Opt. **23**(03), 1–7 (2018).
28. N. V. Chernomyrdin, G. R. Musina, P. V. Nikitin, *et al.*, "Terahertz technology in intraoperative neurodiagnostics: A review," Opto-Electron. Adv. **6**(5), 220071 (2023).
29. N. V. Chernomyrdin, A. S. Kucheryavenko, G. S. Kolontaeva, *et al.*, "Reflection-mode continuous-wave 0.15λ-resolution terahertz solid immersion microscopy of soft biological tissues," Appl. Phys. Lett. **113**(11), 111102 (2018).
30. J. Shi, Y. Y. Wang, T. N. Chen, *et al.*, "Automatic evaluation of traumatic brain injury based on terahertz imaging with machine learning," Opt. Express **26**(5), 6371–6381 (2018).
31. Y. Y. Wang, G. Q. Wang, D. G. Xu, *et al.*, "Terahertz spectroscopic diagnosis of early blast-induced traumatic brain injury in rats," Biomed. Opt. Express **11**(8), 4085–4098 (2020).
32. L. M. Wu, D. G. Xu, Y. Y. Wang, *et al.*, "Horizontal-scanning attenuated total reflection terahertz imaging for biological tissues," Neurophotonics **7**(02), 1 (2020).
33. T. Chiang, R. O. Messing, and W. H. Chou, "Mouse model of middle cerebral artery occlusion," J. Visualized Exp. **48**(48), 2761 (2011).
34. P. A. Ringleb, P. D. Schellinger, C. Schranz, *et al.*, "Thrombolytic therapy within 3 to 6 hours after onset of ischemic stroke," Stroke **33**(5), 1437–1441 (2002).
35. L. Duvillaret, F. Garet, and J. L. Coutaz, "A reliable method for extraction of material parameters in terahertz time-domain spectroscopy," IEEE J. Select. Topics Quantum Electron. **2**(3), 739–746 (1996).
36. S. J. Oh, S. H. Kim, Y. B. Ji, *et al.*, "Study of freshly excised brain tissues using terahertz imaging," Biomed. Opt. Express **5**(8), 2837–2842 (2014).
37. N. Mu, C. Y. Yang, D. G. Xu, *et al.*, "Molecular pathological recognition of freshly excised human glioma using terahertz ATR spectroscopy," Biomed. Opt. Express **13**(1), 222–236 (2022).
38. Y. Y. Wang, T. Notake, M. Tang, *et al.*, "Terahertz-wave water concentration and distribution measurement in thin biotissue based on a novel sample preparation," Phys. Med. Biol. **56**(14), 4517–4527 (2011).
39. T. W. Wang, P. Klarskov, and P. U. Jepsen, "Ultrabroadband THz Time-Domain Spectroscopy of a Free-Flowing Water Film," IEEE Trans. THz Sci. Technol. **4**(4), 425–431 (2014).